Received: 27 March 2020 | Revised: 15 September 2020 | Accepted: 21 September 2020

DOI: 10.1096/fj.202000724R

RESEARCH ARTICLE

THE FASEB JOURNAL

Prolonged podocyte depletion in larval zebrafish resembles mammalian focal and segmental glomerulosclerosis

Kerrin Ursula Ingeborg Hansen[1] | **Florian Siegerist**[1] | **Sophie Daniel**[1] | **Maximilian Schindler**[1] | **Anna Iervolino**[1,2] | **Antje Blumenthal**[1] | **Christoph Daniel**[3] | **Kerstin Amann**[3] | **Weibin Zhou**[4] | **Karlhans Endlich**[1] | **Nicole Endlich**[1]

[1]Institute for Anatomy and Cell Biology, University Medicine Greifswald, Greifswald, Germany

[2]Biogem Research Institute Gaetano Salvatore, Ariano Irpino, Italy

[3]Department of Nephropathology, Institute of Pathology, University of Erlangen-Nürnberg, Erlangen, Germany

[4]Division of Nephrology, Department of Medicine, Icahn School of Medicine at Mount Sinai, New York City, NY, USA

Correspondence
Nicole Endlich, Institute for Anatomy and Cell Biology, University Medicine Greifswald, Friedrich-Loeffler Str. 23c, Greifswald 17487, Germany.
Email: nicole.endlich@uni-greifswald.de

Funding information
Bundesministerium für Bildung und Forschung (BMBF), Grant/Award Number: 01GM1518B

Abstract

Focal and segmental glomerulosclerosis (FSGS) is a histological pattern frequently found in patients with nephrotic syndrome that often progress to end-stage kidney disease. The initial step in development of this histologically defined entity is injury and ultimately depletion of podocytes, highly arborized interdigitating cells on the glomerular capillaries with important function for the glomerular filtration barrier. Since there are still no causal therapeutic options, animal models are needed to develop new treatment strategies. Here, we present an FSGS-like model in zebrafish larvae, an eligible vertebrate model for kidney research. In a transgenic zebrafish strain, podocytes were depleted, and the glomerular response was investigated by histological and morphometrical analysis combined with immunofluorescence staining and ultrastructural analysis by transmission electron microscopy. By intravenous injection of fluorescent high-molecular weight dextran, we confirmed leakage of the size selective filtration barrier. Additionally, we observed severe podocyte foot process effacement of remaining podocytes, activation of proximal tubule-like parietal epithelial cells identified by ultrastructural cytomorphology, and expression of proximal tubule markers. These activated cells deposited extracellular matrix on the glomerular tuft which are all hallmarks of FSGS. Our findings indicate that glomerular response to podocyte depletion in larval zebrafish resembles human FSGS in several important characteristics. Therefore, this model will help to investigate the disease development and the effects of potential drugs in a living organism.

KEYWORDS

FSGS, glomerulus, podocyte injury, zebrafish model organism

Abbreviations: DMSO, dimethyl sulfoxide; dpf, days post fertilization; FFPE, formalin fixed paraffin embedded; FITC, fluorescein isothiocyanate; FSGS, focal and segmental glomerulosclerosis; GBM, glomerular basement membrane; Hpf, hours post fertilization; MTZ, metronidazole; NTR, nitroreductase; PAM, periodic acid methenamine; PAN, puromycin aminonucleoside; PBS, phosphate buffered saline; pcna, proliferating cell nuclear antigen; PEC, parietal epithelial cell; TEM, transmission electron microscopy; ZFIN, Zebrafish Information Network.

1 | INTRODUCTION

Focal segmental glomerulosclerosis (FSGS) is a life-threatening progressive disease with limited therapeutic options often resulting in end stage kidney disease. It is well known that podocyte damage and subsequent depletion are the first steps in the development of FSGS[1] followed by an activation of parietal epithelial cells (PECs). This activation leads to the formation of cellular lesions on the glomerular tuft.[2] Recently, Kuppe and colleagues have shown that upon activation, PECs develop a cuboidal phenotype and are the main cell type in sclerotic lesions.[3] Simultaneously, remaining podocytes lose their complex 3-D morphology, interdigitating podocyte foot processes become broadened as well as flattened which is named foot process effacement.

Since experimental procedures in rodents are not suitable for high-throughput drug screenings, we and others use zebrafish larvae as a simple vertebrate model[4] to study glomerular morphology[5] as well as the permselectivity of the glomerular filtration barrier.[6] Starting at 48 hours past fertilization (dpf), zebrafish larvae develop a single already filtering glomerulus which is connected to a pair of tubules.[4] Analogous to mammals, the glomerular filtration barrier consists of a fenestrated endothelium, the glomerular basement membrane (GBM), and interdigitating podocyte foot processes, which are bridged by an electron-dense slit diaphragm that is formed by homodimerization of the transmembrane protein nephrin.[4] Due to the translucency of the early larvae, the rapid development of the filtration barrier of its simple kidney, its morphology and genetics homologous to mammals, the zebrafish model is ideally suitable for high-throughput drug screenings.[7] As the zebrafish model is easily accessible to fast genetic methods like morpholino-oligonucleotide-mediated knockdowns of genes, the model has been used in a number of studies investigating genetic causes of primary FSGS by generating knockdowns of *nphs1/nphs2*,[8] *cd2ap*,[9] *wt1*,[10] or *inf2*.[11]

To generate a podocyte injury comparable to FSGS, we applied the transgenic nitroreductase/metronidazole (NTR/MTZ) model for cell-specific tissue ablation, first established in zebrafish by Davidson and collegues.[12] In our model of podocyte depletion, the prodrug MTZ is activated exclusively in podocytes expressing the NTR under control of the *nphs2* promotor via the Gal4/UAS-system.[13] Activated MTZ functions as a DNA cross linking agent, which induces selective cell death of podocytes. This leads to rapid onset of proteinuria and edema resembling human nephrotic syndrome.[5,6,14] The aim of this study was to examine the glomerular response upon partial podocyte depletion and to investigate the applicability of this model for human FSGS.

2 | MATERIALS AND METHODS

2.1 | Zebrafish husbandry and MTZ treatment

Zebrafish (Danio rerio) were bred, maintained, and staged as described before.[6] We used the double transgenic strain Tg (*nphs2*:GAL4); Tg (UAS:*Eco.nfsb*-mCherry), ZFIN: ZDB-FISH-160601-2 backcrossed to transparent mitfa$^{w2/w2}$ for at least two generations to generate homozygous double transgenic larvae for all experiments. Larvae express the bacterial enzyme nitroreductase and the fluorescent protein mCherry exclusively in podocytes. Prior to all experiments, larvae were selected for homogenous mCherry expression in the group within the glomerulus. From this selected groups, larvae were randomly assigned to the treatment and control groups. All experiments were performed according to German animal protection law overseen by the "Landesamt für Landwirtschaft, Lebensmittelsicherheit und Fischerei, Rostock" of the federal state of Mecklenburg—Western Pomerania. For drug treatment, 0.1% DMSO was freshly diluted in E3-embryo medium. MTZ (Sigma-Aldrich, St. Louis, MO, USA) was added at a concentration of 80 μmol L^{-1} for all experiments. Controls were treated with 0.1% DMSO-solution only. Treatment was started at 4 dpf and a treatment period of 48 hours was held for all experiments.

2.2 | Histology

Larvae for histological analysis were fixed at 6 dpf and at 9 dpf in 4% paraformaldehyde at 4°C overnight. Glycol methacrylate plastic resin embedding was performed with Technovit 7100 (Kulzer GmbH, Hanau, Germany) as per the manufacturer's instructions. 4 μm transversal sections were made with a Jung RM 2055 rotational microtome (Leica Microsystems, Wetzlar, Germany). H&E and PAM silver staining according to Jones were performed adhering to Technovit 7100 routine staining protocols.

2.3 | Immunofluorescence staining

For *podocin*, *collagen I alpha 1* and *atp1a1* staining, larvae were fixed in 4% paraformaldehyde at 4°C overnight and embedded in paraffin according to the standard protocols. 5 μm sections were made on a Leica SM 200R microtome. After heat-mediated antigen retrieval, sections were incubated with primary antibodies 1:500 polyclonal rabbit anti-podocin (Proteintech, IL, USA) or 1:500 polyclonal rabbit anti-col1a1 (GeneTex, CA, USA) or 1:200 monoclonal mouse anti-*atp1a1* (a6F clone, Developmental

Studies Hybridoma Bank, University of Iowa, deposited by DM Fambrough, Johns Hopkins School of Medicine) at 4°C overnight. For *pcna*, *pax2a* and *laminin* staining, larvae were fixed in 2% paraformaldehyde at 4°C overnight. 30% sucrose in PBS was mixed 1:1 with TissueTek (Sakura Finetek Europe, AV, Netherlands) and used for infiltration for 3 hours at room temperature. Samples were snap-frozen in liquid nitrogen. Between 4-5 µm sections were made on a Microm HM 560 microtome (Thermo Fisher Scientific, MA, USA). After permeabilization with 0.3% Triton X-100 and five washes with PBS, slides were incubated with 1:50 polyclonal rabbit anti-*pcna* (sc-56, Santa Cruz Biotechnology, TX, USA), 1:500 rabbit anti-pax2a (ab229318, abcam), or 1:35 polyclonal rabbit anti-*laminin* (L9393, Sigma-Aldrich) at 4°C overnight. Slides were washed five times in PBS. For all stainings except staining for *atp1a1*, Alexa Fluor 488-, or 647-conjugated goat anti-rabbit IgG F(ab) 2 antibody fragment (Dianova, Hamburg, Germany) were used at 1:300 dilution. For *atp1a1* staining, Cy3-conjugated goat anti-mouse IgG (Jackson ImmunoResearch, PA, USA) was used at a 1:300 dilution. For the staining of human FSGS and control tissue biopsies, anonymized excess tissue of kidney biopsies that was diagnosed by experienced nephropathologists of the Dept. of Nephropathology, University Erlangen-Nürnberg, was used. The use of kidney biopsies from Erlangen has been approved by the Ethics Committee of the Friedrich Alexander University of Erlangen-Nürnberg, waiving the need for retrospective consent for the use of archived excess material (Ref. No. 4415). Briefly, 5 µm sections of FFPE-material was collected on super frost slides, deparaffinized in xylene, and hydrated in an ascending ethanol series. After heat-mediated epitope retrieval in 10 mM citric acid buffer pH6 in a pressure cooker, sections were incubated with the aforementioned *atp1a1* antibody (1:200) and a guinea pig anti *nephrin* antiserum (1:300, gpN2, Progen, Heidelberg, Germany) at 4°C overnight. After five washes in PBS the primary antibodies were detected using 1:800 Cy3-conjugated donkey anti guinea pig and 1:800 Alexa Fluor 488-conjugated goat anti mouse antibodies Dianova, Hamburg, Germany). In all stainings, cell nuclei were counterstained with 0.1 mg/mL DAPI (4′,6-Diamidine-2′-phenylindole dihydrochloride, Sigma, MO, USA) for 20 minutes. After one wash with PBS, and with A. dest, slides were mounted with Mowiol for microscopy (Roth, Karlsruhe, Germany). Immunofluorescence micrographs were acquired with a TCS SP5 confocal laser scanning microscope (C-LSM) using the 63x, 1.4 NA oil immersion objective (Leica Microsystems, Wetzlar, Germany). Brightfield images were acquired with an Olympus BX50 light microscope using the 40x, 0.6 NA objective (Olympus, Hamburg, Germany). ImageJ V1.51f (Wayne Rasband, National Institutes of Health, USA) was used for all morphometric measurements, the cell counter plugin was used to count pax2a$^+$ cells on the glomerular tuft.

2.4 | Transmission electron microscopy

Larvae collected at early 9 dpf were fixed in 4% glutaraldehyde, 1% paraformaldehyde, and 1% sucrose in 0.1 M HEPES at 4°C overnight and embedded in EPON 812 (Serva, Heidelberg, Germany) as per the manufacturer's instructions. Semithin (500 nm) and ultrathin sections (70 nm) were made on an Ultracut UCT microtome (Leica Microsystems, Heidelberg, Germany). Semithin sections were stained with methylene blue. UItrathin sections were placed on copper grids, contrasted with 5% uranyl acetate for 5 minutes and with Sato's lead stain for 5 minutes. Images were acquired with a LIBRA 120 TEM (Carl Zeiss GmbH, Oberkochen, Germany) with an anode voltage of 80 kV.

2.5 | Statistical analysis

GraphPad prism V5.01 (GraphPad Software, CA, USA) was used for all statistical analyses. Gaussian distribution was checked by Kolmogorov-Smirnov testing. If passed, Student's t test was used for significance testing and mean was given in the results. For statistical testing of nonparametric data, Mann-Whitney U test was applied, and median was used. P-values lower 0.05 were considered statistically significant.

3 | RESULTS

We used the transgenic zebrafish strain *Cherry* (Tg(*nphs2*:GAL4); Tg(UAS:Eco.nfsb-mCherry); mitfa$^{w2/w2}$ on AB-Tü background) for all experiments. *Cherry* larvae express the bacterial NTR together with the red fluorescent protein mCherry under control of a podocyte-specific GAL4-driver (Figure 1A). After administration of the prodrug MTZ to the medium, MTZ is taken up by the cells and converted into a cytotoxic agent uniquely in NTR-expressing cells, in this case podocytes (Figure 1A′). MTZ induces interstrand DNA crosslinking and subsequent apoptosis in a concentration dependent manner,[14,15] resulting in areas with denuded GBM due to the detachment of affected podocytes. To generate conditions comparable to the situation found at the onset of FSGS in mammals, we used a low dose of MTZ to deplete only a subset of podocytes. Cherry larvae were treated with low-dose MTZ (80 µmol L^{-1} in 0.1% DMSO) or with 0.1% DMSO as a control beginning at 4 dpf. MTZ and DMSO was washed out after 48 hours of treatment.

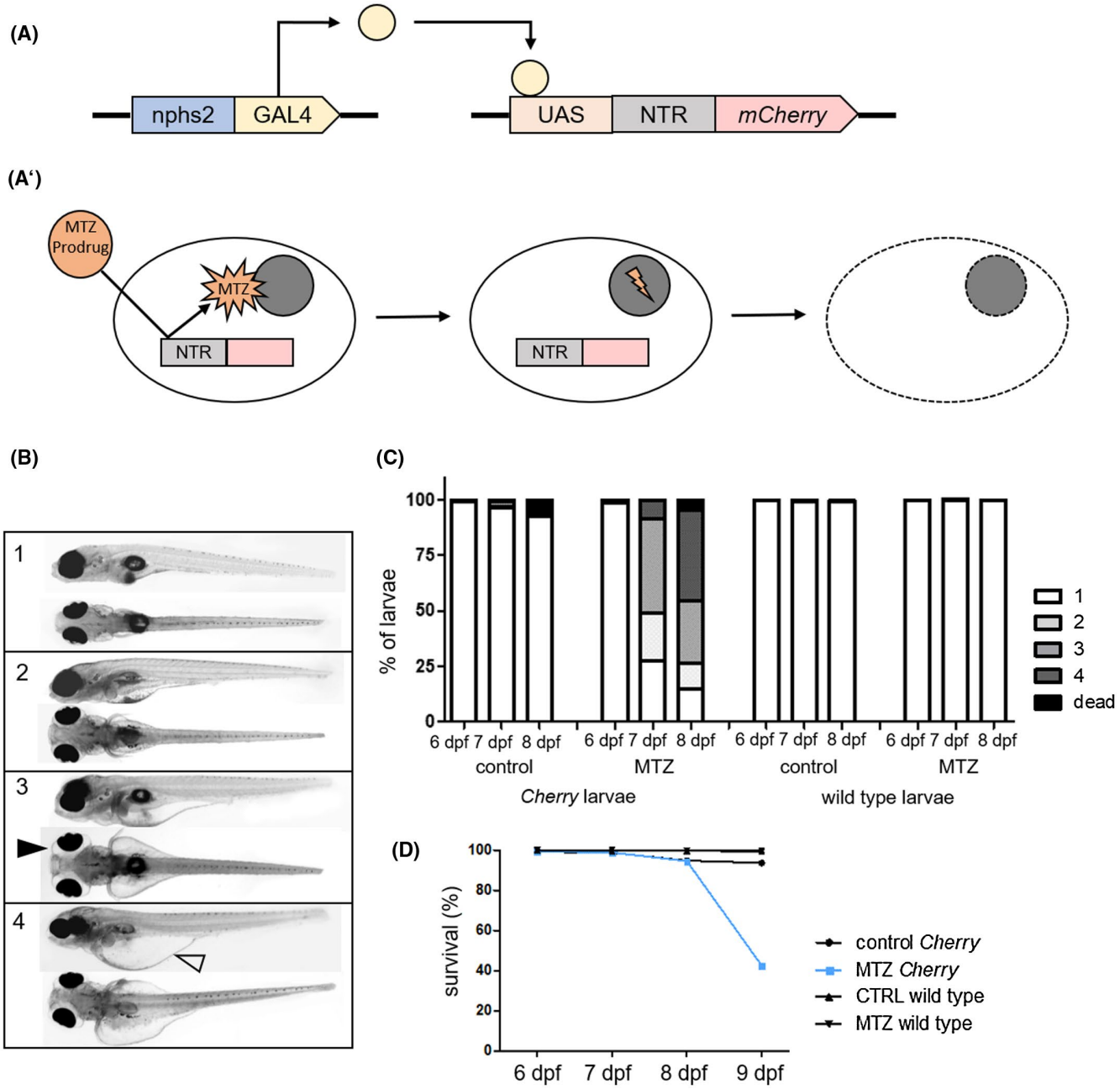

FIGURE 1 A, Schematically shows gene expression in the used transgenic zebrafish line. Gal4 is expressed under the *nphs2* promotor. After binding to its specific recognition sequence UAS (upstream activation sequence), it activates the expression of a bacterial nitroreductase (NTR) and the red fluorescence protein *mCherry*. A′ shows a scheme of how MTZ is activated by NTR and subsequently induces DNA damage, which leads to apoptosis. B shows representative micrographs of 8 dpf zebrafish larvae to demonstrate the grading of developing edema after podocyte depletion. (1) no edema, (2) mild edema, (3) medium edema, and (4) severe edema. The black arrowhead exemplary indicates periocular edema, the blank arrowhead indicates abdominal edema. The graph in C shows relative distributions of phenotypes in n = 251 control-treated and n = 275 MTZ-treated *Cherry* larvae in four individual experiments and in n = 250 control-treated and n = 250 MTZ-treated wild-type larvae. As visualized in the diagram in D, survival rates of podocyte-depleted *Cherry* larvae are similar to controls until an abrupt decrease at 9 dpf

We observed edema of different severity in larvae treated with low-dose MTZ which was graded into four categories starting from 1 (no edema) to 4 (severe whole body edema with bent body axis) as shown in representative images of 8 dpf zebrafish larvae in Figure 1B. We found that MTZ-treated *Cherry* larvae developed edema 1 day after MTZ-washout (7 dpf). At 8 dpf, 69% (of total n = 275) of living MTZ-treated *Cherry* larvae showed medium to severe edema formation (Figure 1C) and 51% of MTZ-treated *Cherry* larvae finally died at 9 dpf (Figure 1D). In contrast to that, only 10% (of n = 251) of the control-treated *Cherry* larvae showed edema of any severity or died during the observation time

(Figure 1C,D). In contrast to that, nitroreductase-negative non-transgenic wild-type larvae (AB-Tü strain) treated with either 80 μmol L^{-1} MTZ in 0.1% DMSO or 0.1% DMSO vehicle control did not show significant edema or decreases viability (Figure 1C,D).

To indirectly quantify proteinuria and to determine the integrity of the glomerular filtration barrier, we intravenously injected far-red fluorescent low molecular weight dextran (10 kDa conjugated to Alexa Fluor-647) together with green fluorescent high molecular weight dextran (500 kDa, FITC), directly after MTZ-washout. 0.5 and 19 hours after the injection of the dextrans, we determined the intravascular fluorescence in the caudal vein by in vivo confocal laser scanning microscopy (C-LSM), shown in Figure 2A. The fluorescence of FITC decreased by 59% in MTZ-treated larvae after 19 hours ($P = .0002$ compared to the controls; n = 31), whereas the fluorescence of FITC in controls did only decline slightly (Figure 2B). Moreover, immunofluorescence staining with a polyclonal *podocin* antibody showed a significant reduction in MTZ-treated larvae in comparison to controls, which displayed a regular and strong linear staining pattern along the glomerular capillaries (Figure 2C,D).

Transmission electron microscopy (TEM) of MTZ-treated larvae at 9 dpf revealed disintegrated cells along the GBM localized close to podocytes (Figure 2E). The foot processes of remaining podocytes of MTZ-treated larvae were severely effaced, whereas controls the exhibited intact podocytes with regular foot processes that were bridged by an electron dense slit membrane (magnifications in Figure 2E).

Furthermore, histologic analysis of formalin-fixed and plastic-embedded larvae showed a reduced glomerular cell density in MTZ-treated larvae compared to controls (median: 0.014 nuclei per μm^2 in MTZ-treated larvae vs 0.022 nuclei per μm^2; $P = .0011$; n = 24) (Figure S1A,B). It remained still reduced after 3 days of regeneration (0.0161 nuclei per μm^2 vs 0.0325 nuclei per μm^2 in controls at 9 dpf; $P = .0003$; n = 24), although the absolute cell numbers at the capillaries of MTZ-treated larvae increased to a level similar to controls (Figure S1B,C). Numbers of podocytes per glomerular cross-section determined by TEM remained significantly reduced (mean: 9.0 vs 13.25 at 9 dpf; $P = .0043$; n = 17) (Figure S1D). Moreover, we found that the Bowman's capsules were enlarged after MTZ-treatment, which was determined as the area of the largest of the consecutive glomerular serial cross-sections for each larva. At 6 dpf, the mean was 1043 μm^2 after MTZ treatment compared to 538 μm^2 in controls (Figure S1E, $P = .0008$, n = 24). The difference was even higher at 9 dpf (1085 μm^2 in MTZ-treated larvae vs 374 μm^2, $P = .0019$, n = 24).

In podocyte-depleted larvae, distinct severities of podocyte impairment could be discriminated by TEM: In 45% (5 of n = 11) of MTZ-treated larvae, glomeruli showed a uniform electron dense GBM, well fenestrated endothelial cells similar to controls, but a severe foot process effacement (Figure 3A). Only a few capillaries showed normal foot processes. Moreover, dilatations of the sub-podocyte space were frequently found (asterisk in Figure 3A). In 36% (4/11) of MTZ-treated larvae, no typical foot processes of podocytes were visible. As shown in Figure 3B, visceral epithelial cells were instead showing tight junctions and microvillous transformation. 18% (2/11) of MTZ-treated larvae showed a phenotype of intermediate severity that showed characteristics of both previously described. Total numbers of local electron-dense contacts to neighboring cells per visceral epithelial cell were increased from 0.29 in controls to 2.2 tight junctions per cell in MTZ-treated larvae ($P = .0002$, n = 20) (Figure 3B,C).

Histomorphologic analysis showed a thickening of the PEC-layer that progressed between 6 to 9 dpf (Figure 4A). After MTZ washout (6 dpf), mean thickness of PECs was 0.9 μm in controls and 1.11 μm in podocyte-depleted larvae ($P = .0043$; n = 24). At 9 dpf, it was 0.78 μm in controls and 3.96 μm after MTZ treatment ($P = .0001$; n = 24) (Figure 4B). Under baseline conditions, PECs show very little proliferation but become more replicative after injury-induced activation. Immunostaining for *proliferating cell nuclear antigen* (*pcna*), an antigen only present during S-phase in cellular replication, revealed proliferating PECs only in podocyte-depleted larvae (Figure 4C).

To investigate whether these cuboidal cells on the glomerular tuft were of PEC/tubular-origin, we immunostained with a polyclonal antibody for the transcription factor *pax2a* which is a marker of the proximal tubular neck segment and parietal epithelial cells in the zebrafish pronephros.[16] As shown in the C-LSM micrograph in Figure 4D, proximal tubule cells and PECs where strongly *pax2a*-positive under baseline conditions. Upon podocyte-depletion we found an increase of the *pax2a* protein abundance on the parietal leaf of Bowman's space. Additionally, the de-novo appearing cuboidal cells on the glomerular tuft also expressed strongly *pax2a,* whereas podocytes were *pax2a* negative. Figure 4E shows counts of *pax2a*-positive cells on the glomerular tuft in MTZ-treated larvae and in controls. After podocyte depletion, a statistically significant number of $pax2a^+$ cells were recruited to the glomerular tuft.

To further discriminate the origin of these cuboidal $pax2a^+$ cells on the glomerular tuft, we additionally stained for the Na^+-K^+-ATPase subunit alpha 1 (*atp1a1*) using a monoclonal antibody which in mammalian kidneys is a tubular marker and under baseline conditions not expressed in the glomerulus or PECs as shown in the immunohistochemistry micrographs of the protein atlas database (http://proteinatlas.org) in Figure S2. To verify that *atp1a1* is expressed in the proximal tubules and not in healthy PECs in zebrafish as well, we stained sections of MTZ-treated and control zebrafish larvae for *pax2a* and *atp1a1* simultaneously. A co-expression

of both markers was found, as shown in Figure 5A. Similar to mammals, proximal tubule cells where strongly expressing *atp1a1* under control and diseased conditions in the basolateral cell membrane. Only after podocyte-depletion, activated prismatic PECs were also found *atp1a1*-positive. Additionally, we frequently found double positive cuboidal *atp1a1* and *pax2a* positive cells on the glomerular tuft (Figure 5B).

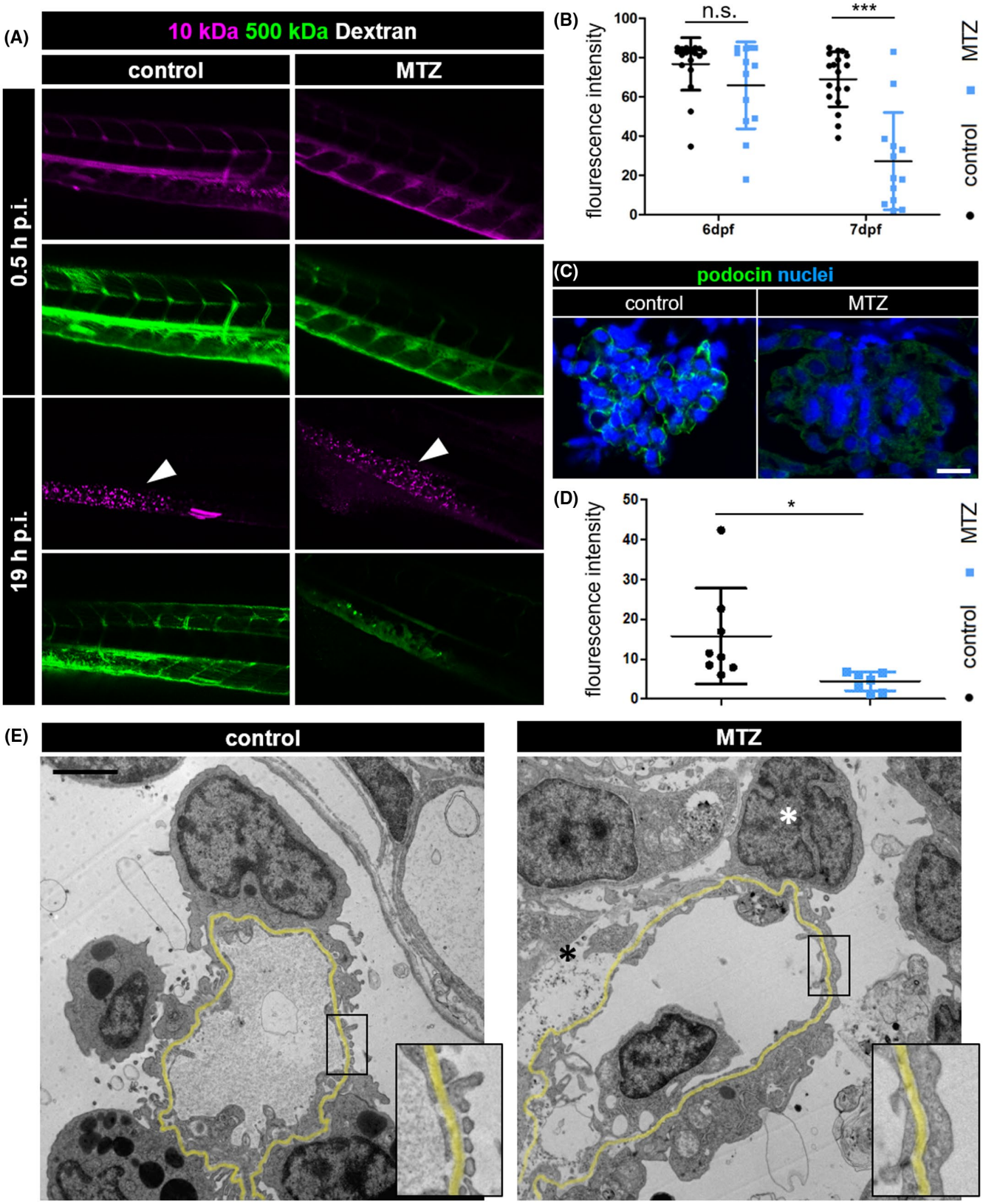

FIGURE 2 A, Confocal laser scanning micrographs of podocyte-depleted and control larvae 0.5 and 19 hours after injection with a mixture of FITC-conjugated 500 kDa and Alexa Fluor647-conjugated 10 kDa dextran directly after metronidazole washout. Notice the decrease of 500 kDa dextran in podocyte-depleted larvae, whereas 10 kDa dextran accumulates in the tissue as shown in the caudal fin (white arrowheads). As shown in graph B, fluorescence intensity of FITC measured in the caudal vein was significantly lower in podocyte-depleted larvae 19 hours after dextran injection. C, The linear staining pattern of podocin 3 days after vehicle treatment in controls while the signal is greatly reduced in podocyte-depleted larvae. The scale bar represents 10 μm. D, Quantification of these differences by fluorescence intensity. Transmission electron micrographs of 9 dpf control larvae in panel E reveal a normal morphology with fine foot processes connected by a slit diaphragm, whereas podocyte foot processes in MTZ-treated larvae are broadly effaced, as shown in detail in the magnifications at the bottom right corner of each image. The white asterisk labels the nucleus of a remaining podocyte after MTZ treatment. Remnants of an apoptotic podocyte are marked by the black asterisk. The GBM is highlighted in yellow. Scale bar represents 2 μm

To find out whether this finding was restricted to the zebrafish model only or rather a conserved mechanism, we stained FFPE sections of kidney biopsies of n = 4 patients with biopsy-proven FSGS and of n = 4 controls (tumor-free excess tissue of tumor nephrectomies with healthy appearing histology) for *atp1a1* and the podocyte-marker *nephrin*. As expected, in the healthy controls, *atp1a1* expression was absent in cells of the glomerular tuft and PECs and began right at the PEC-proximal tubular interface (arrowhead in Figure 5C). In contrast to that, activated PECs in the FSGS biopsies showed *atp1a1* positivity (arrow in Figure 5C). This phenomenon could be seen in at least one glomerulus in three out of four of the examined biopsies (Figure S3).

Another feature of human FSGS is the presence of adhesions of the parietal and visceral epithelial layer that are formed by activated PECs to the denuded areas of the GBM. In line with the previous findings, we found that in glomeruli of podocyte-depleted larvae, adhesions between the activated parietal and visceral glomerular cell layer were visible in H&E sections (Figure 6A) and TEM micrographs (Figure 6B). Since podocyte loss in humans is followed by progressive scarring of the glomerulus, we investigated extracellular matrix deposition in podocyte-depleted zebrafish larvae. While Jone's stain showed slight accumulation of silver-positive material on the glomerular tuft at 9 dpf (Figure 4A), a strong accumulation of laminin was seen (Figure 6C) with significant GBM-thickening (Figure 6D). However, we could not detect the accumulation of *collagen I* at 9 dpf (Figure S4).

Following podocyte injury and using classic histology and TEM, we identified immigrating neutrophils and macrophages within Bowman's capsule only in podocyte-depleted larvae and not in healthy control animals (Figure S5).

4 | DISCUSSION

It has been shown previously that the main reason leading to the histologic pattern of FSGS is injury and subsequent loss of podocytes. Regardless of the initial cause of podocyte injury, may it be genetic, by endogenous circulating podocytotoxic factors or directly exogenously toxic, the relationship between podocyte depletion and glomerulosclerosis has been shown in humans,[17-19] as well as in animal models such as transgenic mouse models of podocyte ablation,[20,21] puromycin aminonucleoside (PAN)-treated rats[22] and podocyte ablation by diphtheria toxin injection in transgenic rats expressing the human diphtheria toxin receptor exclusively in podocytes.[23] Unfortunately, these model organisms are not easily usable in high-throughput assays and even in the era of CRISPR/Cas9 genetic manipulation is rather difficult and time-consuming. In the zebrafish model, the small larval size and conserved morphology of the pronephros offers a general applicability for high-throughput assays as larvae can easily be treated and screened in the 96-well format as it has been shown before for modulators of polycystic kidney disease using a morpholino-based genetic zebrafish model[24] or a developmental drug nephrotoxicity assay[25] which both used pronephric morphometry as the primary readout.

To analyze the glomerular response to podocyte depletion in zebrafish and investigate the suitability of larval zebrafish as a model for human FSGS, a targeted model of podocyte depletion was needed. PAN has been shown to induce podocyte injury in larval zebrafish, but since it has to be intravenously injected, it is not directly eligible for high-throughput screenings in which minimal hands-on time is a prerequisite for scalability.[9] Another available method of podocyte depletion is laser-induced injury, but spatial specificity of the damage requires ablation of single cells, so treatment of higher counts of larvae at the same time would not be possible.[26] Non-transgenic attempts to induce podocyte injury by adding reagents to the water have not been successful for the effect was either minimal or not limited to podocytes.[27]

To date the only inducible model of podocyte depletion that combines the ease of adding a reagent to the medium with the advantage of cell-specific ablation is the NTR/MTZ model.[5,14] In this study, we chose a short treatment with low-dose MTZ to deplete a subset of podocytes so that larvae survived long enough to investigate glomerular response and adaption to injury.

As described before, MTZ-treated larvae developed periocular edema, which is a hallmark for hypoproteinemic proteinuria.[14] Wild-type larvae did not develop significant

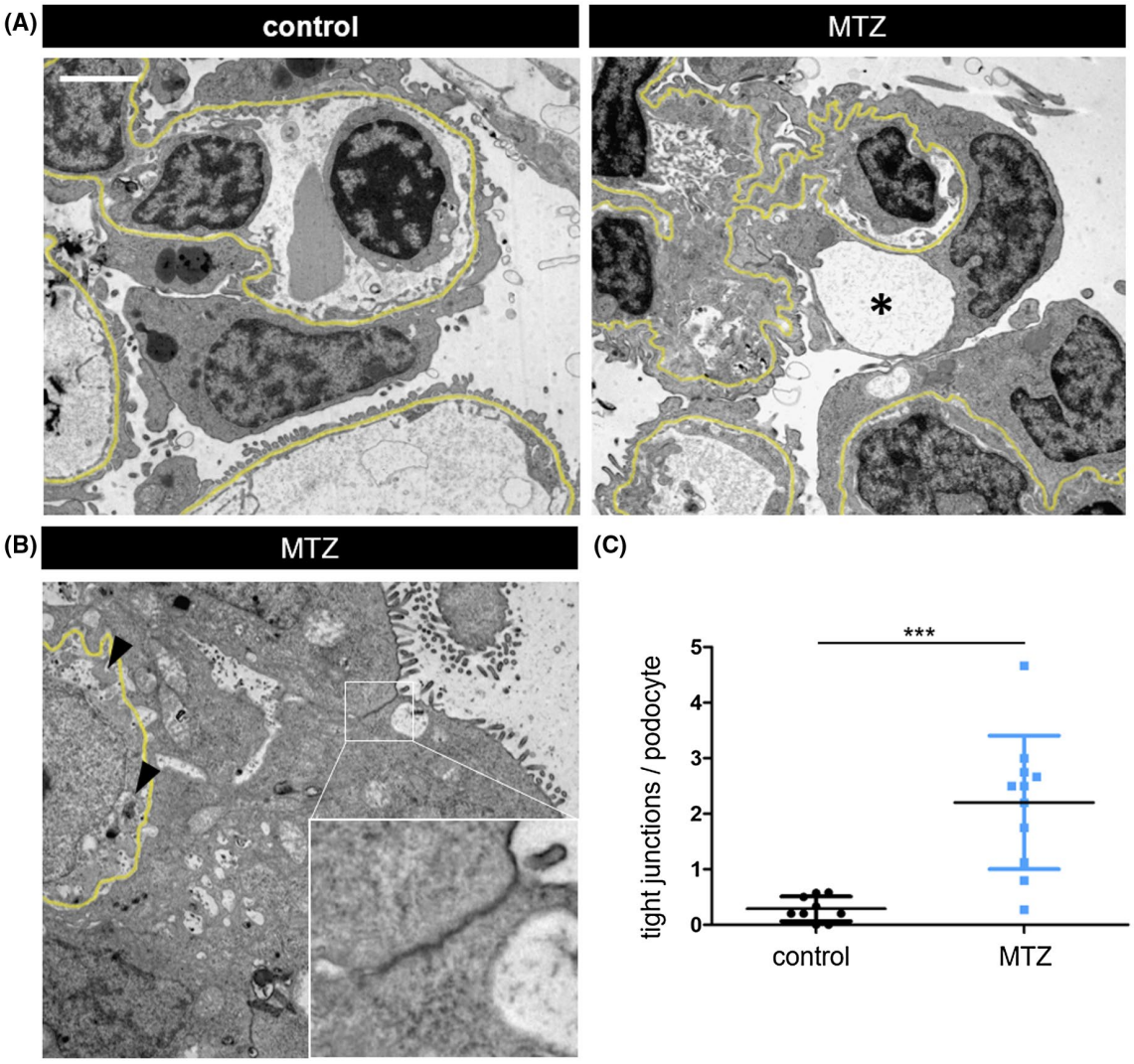

FIGURE 3 Contrasting intact podocyte foot processes in control larvae, podocyte-depleted glomeruli displayed signs of podocyte impairment as shown in the representative micrographs in A. Adjacent to a capillary displaying almost normal morphology; podocyte foot process effacement and subpodocyte space, pseudocysts (asterisk) can be seen. Scale bar represents 2 μm. MTZ-treated larvae showed markedly increased tight junctions between remaining podocytes in n = 20 larvae (B, C). An electron-dense tight junction is shown in detail in the bottom right corner of the picture in B. Black arrowheads accentuate loss of fenestration and cellular integrity of the capillary endothelium

numbers of edema, indicating NTR-dependency and specificity of the phenotype. Furthermore, we verified the loss of permselectivity of the glomerular filtration barrier using clearance of fluorescent-labeled high molecular weight dextran from the vasculature which under healthy conditions is retained in the blood plasma by the GFB. Three days after MTZ washout, some non-detached podocytes were found on the glomerular capillaries that showed severe foot process effacement and reduction of the expression of the slit membrane protein *podocin* as a sign of persistent podocyte injury. An increase of tight junctions between neighboring podocytes can be interpreted as a mechanism to prevent detachment from the GBM under increased mechanical forces and filtration which has been described extensively in human patients and mammalian models.[28,29]

Although the size of the glomerular tuft significantly increased, the total number of podocytes per glomerular cross section remained significantly lower than in controls, indicating cellular hypertrophy of remaining podocytes. Previous work has shown that insufficient podocyte-hypertrophy and subsequent mechanical stress leads to the development of sub-podocyte space pseudocysts preceding podocyte detachment.[30] Furthermore, increased filtration in the sub-podocyte space has been suggested to play an important role in the regulation of glomerular permeability.[31]

Another key feature of mammalian FSGS is the activation of PECs which contribute to fibrotic lesions, as it has nicely been shown by Smeets and colleagues,[32] and thickening of Bowman's capsule.[33] By analyzing the *pax2* expression, Ohtaka et al and Dijkman et al furthermore showed that cells

on the parietal-visceral interface contribute to cellular lesions in human FSGS.[34,35]

In our model, PECs started to proliferate and changed their morphology toward a cuboidal, microvillous phenotype following activation due to podocyte detachment. These findings strongly support the hypothesis that upon podocyte-depletion, flat PECs transform to cuboidal PECs, as it has recently been shown by Kuppe et al.[3] Together with the

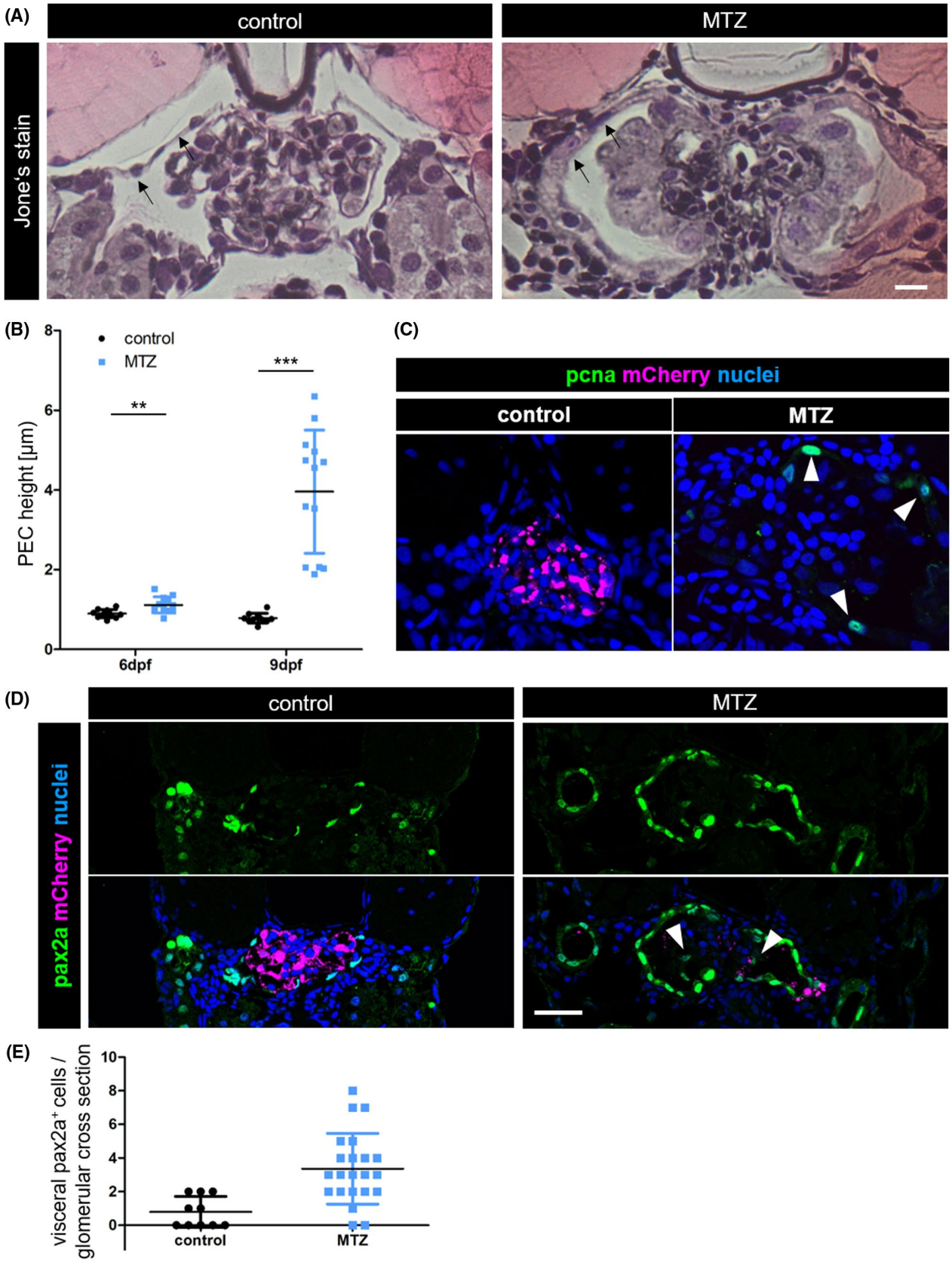

FIGURE 4 Panel A representative micrographs of Jone's-stained plastic sections of podocyte-depleted and control larvae. Black arrows point at the PEC layer. The scale bar represents 10 μm. The graph in B shows the result of PEC height measurements in H&E-stained plastic sections of n = 25 podocyte-depleted and n = 23 control larvae. A statistically significant increase is visible in podocyte-depleted larvae directly after, and 3 days after treatment. The micrographs in panel C show *pcna*-staining of larvae collected at 9 dpf. Expression of *mCherry* labels podocytes. Podocyte-depleted larvae show *pcna*-positivity of PECs (white arrowheads). Panel D demonstrates *pax2a*-positive PEC-nuclei under baseline conditions with increased expression of *pax2a* in cuboidal PECs and cuboidal cells on the glomerular tuft 3 days after podocyte depletion (white arrowheads). The scale bar represents 25 μm. The graph in E shows quantification of these differences

typical cytomorphology and the expression of *pax2a, atp1a1,* and not *podocin* (no podocin protein in immunofluorescence and no podocin promotor activity as shown by missing transgene expression), we characterized them as cuboidal proximal-tubule like PECs that covered the denuded areas of the GBM in the most severely injured 36% of MTZ-treated larvae, which fits previous findings in a murine model of collapsing FSGS.[36] Furthermore, using immunofluorescence in FSGS biopsies, we could show that the presence of *atp1a1* was not restricted to the model we used but a general and conserved mechanism as the pattern of *atp1a1* expression in MTZ-treated zebrafish larvae strongly resembled the situation found in human FSGS patients.

In contrast to that, other groups have suggested that PECs are recruited to the glomerular tuft and replace podocytes.[37,38] Another work additionally mentions attachment of PECs to the apical sides of podocytes after activation and both propose extracellular matrix conglomerates in FSGS to be synthesized by PECs as we have demonstrated in our model.[36,39] Still, the pathways involved in PEC activation following podocyte injury remain incompletely understood. Romoli et al recently proposed *cxcl12* derived by podocytes into Bowman's Space as a quiescence signal to PECs.[40] A study performed by Kuppe et al in 2015 focused on the role of PECs in secondary FSGS in humans. It revealed that cells expressing the marker *anxa3* for all PECs and the PEC matrix marker *lkiv69* were involved in all stages of secondary FSGS, whereas the PEC activation markers *cd44* and *krt19* were expressed in cellular lesions, but only rarely in sclerotic lesions. The findings where independent of the underlying glomerular disease, indicating a common cellular pathway in the development of sclerotic lesions.[41]

Although zebrafish larvae have the general ability to develop sclerosis,[42] they seem to develop remarkably little fibrosis and instead regenerate tissue as shown for cardiomyocytes.[43] Expression analysis of the prevalent extracellular matrix component collagen 1, which is expressed in tissues of the musculoskeletal system of healthy individuals, does not seem to detect sclerotic lesions sensitively, for we could not detect it in the glomerulus despite clear accumulation of laminin. Since accumulation of laminin, in combination with other extracellular matrix components, directly causes a thickening of the GBM, GBM width is equal to quantification of laminin staining as a readout.

As a potential readout for potential positive influence of screened drugs on the disease cause two different approaches can be chosen: First, an aim of analysis could be the impact of potential drugs on the number of *atp1a1*- or *pax2a*-positive cells on the glomerular tuft as an indicator of involvement of cuboidal PECs contribute to sclerotic lesions. At least for *pax2a*, a number of fluorescent reporter strains are available which can be readily used to automate detection of intraglomerular *pax2a* expression and, therefore, quantification of recruitment of disease-accelerating proximal-tubule like cuboidal PECs.

Second, as a more direct marker for disease progression, effects on proteinuria using transgene reporter lines like the eGFP-labeled vitamin D binding protein line could be used. In this model strains, 78 kDa eGFP-labeled vitamin D-binding protein is synthesized in hepatocytes and secreted to the blood plasma. As in healthy conditions, the eGFP-fusion cannot pass the GFB freely, its intravascular fluorescence intensity directly reflects the function of the GFB as we have shown for the NTR-MTZ model before.[6] Therefore, the slope of the intravascular eGFP-intensity decrease directly correlates with progression of proteinuria and is ideal as a primary screening readout. In 2020, Steenbergen et al presented a similar approach with easier imaging but more complicated iv injections where they used intravascular FITC-inulin clearance as a readout in a high-content zebrafish drug screening pipeline for automated imaging in the 96 well format.[44]

Taken together, here we have shown that podocyte depletion in zebrafish larvae is a versatile model that resembles the clinical and histological appearance of human FSGS in important characteristics such as proteinuria, development of edema, formation of viscero-parietal adhesions, PEC activation and -proliferation as well as deposition of extracellular matrix. Our results establish a basis not only for the use of the FSGS-like disease in zebrafish as a model for further studies investigating the pathogenesis of FSGS, but also for assessing the effects of potential drugs on disease development in a vertebrate model suitable for high-throughput experiments.

Additionally, we have found strong evidence, that the development of glomerular sclerotic lesions by the activation of proximal tubulus-like PECs is a conserved process that is present across vertebrate species.

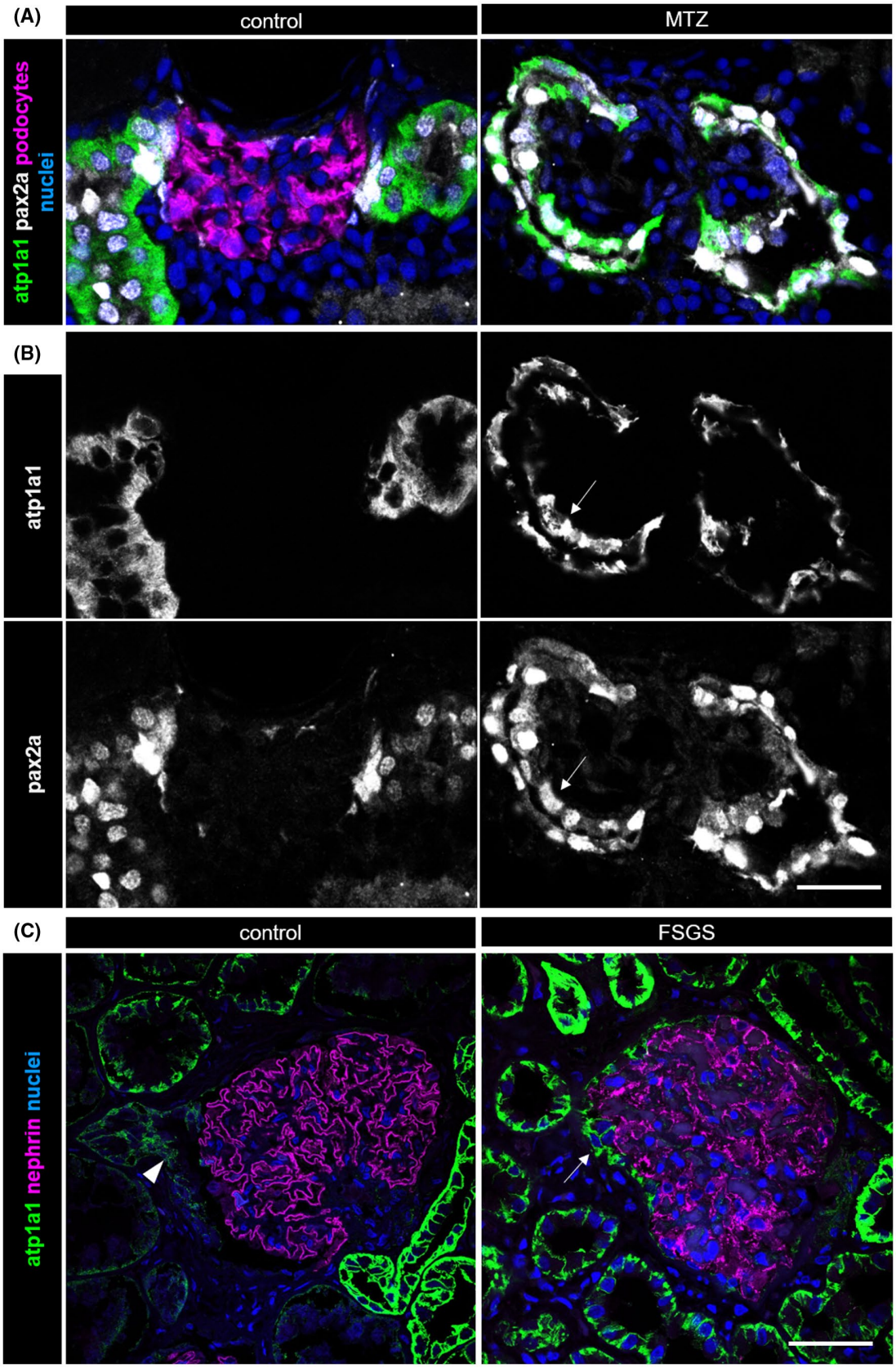

FIGURE 5 Co-expression of *atp1a1* and *pax2a* in proximal tubule cells of 9 dpf zebrafish larvae is shown in A. Panel B shows *atp1a1* expression and *pax2a* expression separately. It is limited to the proximal tubule in control larvae; whereas in podocyte-depleted larvae, it is also found in activated parietal epithelial cells and on the glomerular tuft (white arrows). The scale bar represents 20 μm. The micrographs in C exemplary show *atp1a1* expression in a human glomerulus under healthy conditions, where it is limited to the tubule (white arrowhead), and in a patient with FSGS. Notice *atp1a1* positivity of cells on the glomerular capillaries in FSGS, highlighted by the white arrow. *Nephrin* expression marks podocytes. The scale bar represents 50 μm

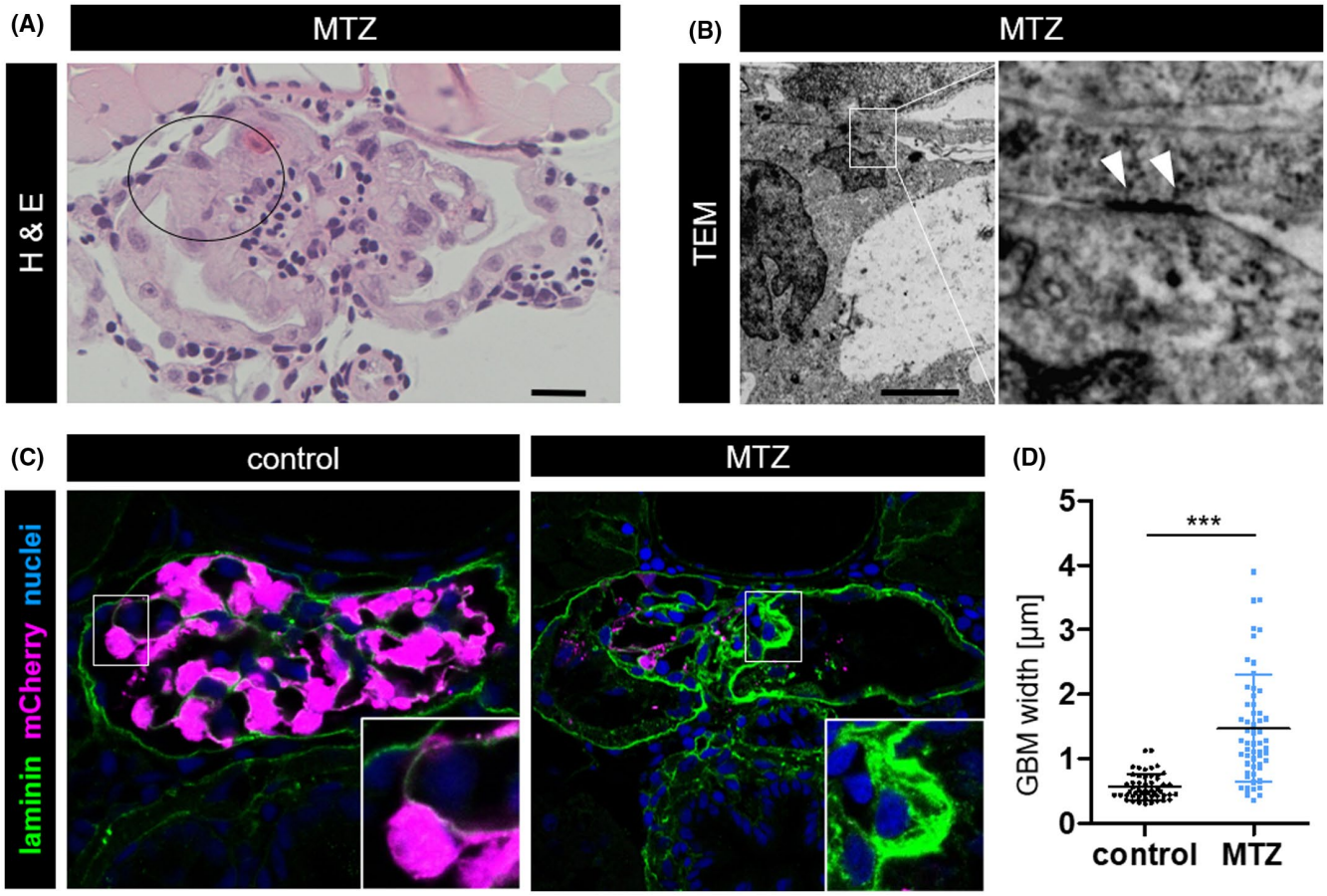

FIGURE 6 A, Parieto-visceral adhesion in an H&E-stained plastic section. Scale bar represents 10 µm. The transmission electron micrograph shown in picture B further characterizes one adhesion. Scale bar represents 2 µm. White arrowheads highlight local electron-dense parieto-visceral contacts in the magnification of B. C, Immunostaining for laminin in podocyte-depleted and control larvae at 9 dpf. A significant deposition of laminin on the glomerular tuft can be noticed as shown in the inserts. *mCherry* expression labels podocytes. The graph in D quantifies the thickness of the laminin-layer within the GBM measured orthogonally as the full width at half maximum. Podocyte-depleted larvae showed statistically significant increased laminin-deposition as measured in five randomly picked capillaries in each three consecutive glomerular cross-sections of n = 5 podocyte-depleted and n = 6 control larvae

ACKNOWLEDGMENTS

This work was supported by three scholarships of the Gerhard Domagk program of the University Medicine Greifswald to KH, FS, and SD and by a grant of the Federal Ministry of Education and Research (BMBF, grant 01GM1518B, STOP-FSGS) to NE This work was generously supported by the Südmeyer fund for kidney and vascular research ("Südmeyer-Stiftung für Nieren- und Gefäßforschung") and the Dr Gerhard Büchtemann fund, Hamburg, Germany. The authors thank Mandy Weise and Oliver Zabel for excellent technical assistance. Open access funding enabled and organized by Projekt DEAL. All authors declare no conflicts of interest.

AUTHOR CONTRIBUTIONS

K. Ursula Ingeborg Hansen, F. Siegerist, S. Daniel, M. Schindler, A. Iervolino, and A. Blumenthal established methods and performed experiments; K. Ursula Ingeborg Hansen, F. Siegerist, K. Endlich, and N. Endlich planned experiments, analyzed and interpreted data; W. Zhou established the transgenic lines used in the study; C. Daniel and K. Amann contributed selected human kidney biopsies of FSGS and control cases. All authors reviewed and approved the final version of the manuscript.

REFERENCES

1. Kriz W. Progressive renal failure—inability of podocytes to replicate and the consequences for development of glomerulosclerosis. *Nephrol Dial Transplant*. 1996;11:1738-1742.
2. D'Agati VD, Fogo AB, Bruijn JA, Jennette JC. Pathologic classification of focal segmental glomerulosclerosis. A working proposal. *Am J Kidney Dis*. 2004;43:368-382.
3. Kuppe C, Leuchtle K, Wagner A, et al. Novel parietal epithelial cell subpopulations contribute to focal segmental glomerulosclerosis and glomerular tip lesions. *Kidney Internat*. 2019;96:80-93.
4. Drummond IA. Kidney development and disease in the zebrafish. *J Amer Soc Nephrol*. 2005;16:299-304.
5. Siegerist F, Blumenthal A, Zhou W, Endlich K, Endlich N. Acute podocyte injury is not a stimulus for podocytes to migrate along

the glomerular basement membrane in zebrafish larvae. *Sci Rep*. 2017;7:43655. Accessed May 2017. https://www.nature.com/articles/srep43655.
6. Siegerist F, Zhou W, Endlich K, Endlich N. 4D in vivo imaging of glomerular barrier function in a zebrafish podocyte injury model. *Acta Physiol*. 220 2016;(1):167–173.
7. MacRae CA, Peterson RT. Zebrafish as tools for drug discovery. *Nat Rev Drug Discovery*. 2015;14:721-731.
8. Kramer-Zucker AG, Wiessner S, Jensen AM, Drummond IA. Organization of the pronephric filtration apparatus in zebrafish requires Nephrin, Podocin and the FERM domain protein Mosaic eyes. *Dev Biol*. 2005;285:316-329.
9. Hentschel DM, Mengel M, Boehme L, et al. Rapid screening of glomerular slit diaphragm integrity in larval zebrafish. *Am J Physiol Renal Physiol*. 2007;293:F1746-F1750.
10. Perner B, Englert C, Bollig F. The Wilms tumor genes wt1a and wt1b control different steps during formation of the zebrafish pronephros. *Dev Biol*. 2007;309:87-96.
11. Sun H, Al-Romaih KI, MacRae CA, Pollak MR. Human kidney disease-causing inf2 mutations perturb rho/dia signaling in the glomerulus. *EBioMedicine*. 2014;1:107-115.
12. Davison JM, Akitake CM, Goll MG, et al. Transactivation from Gal4-VP16 transgenic insertions for tissue-specific cell labeling and ablation in zebrafish. *Dev Biol*. 2007;304:811-824.
13. Asakawa K, Kawakami K. Targeted gene expression by the Gal4-UAS system in zebrafish. *Dev Growth Differ*. 2008;50:391-399.
14. Zhou W, Hildebrandt F. Inducible podocyte injury and proteinuria in transgenic zebrafish. *J Amer Soc Nephrol*. 2012;23:1039-1047.
15. Knox RJ, Friedlos F, Jarman M, Roberts JJ. A new cytotoxic, DNA interstrand crosslinking agent, 5-(aziridin-1-yl)-4-hydroxylamino-2-nitrobenzamide, is formed from 5-(aziridin-1-yl)-2,4-dinitrobenzamide (CB 1954) by a nitroreductase enzyme in Walker carcinoma cells. *Biochem Pharmacol*. 1988;37:4661-4669.
16. Miceli R, Kroeger P, Wingert R. Molecular mechanisms of podocyte development revealed by zebrafish kidney research. *Cell Develop Biol*. 2014;3:1–7.
17. Kriz W, Lemley KV. The role of the podocyte in glomerulosclerosis. *Curr Opin Nephrol Hypertens*. 1999;8:489-497.
18. Bertram JF, Douglas-Denton RN, Diouf B, Hughson MD, Hoy WE. Human nephron number. Implications for health and disease. *Pediatr Nephrol*. 2011;26:1529-1533.
19. Shankland SJ. The podocyte's response to injury. Role in proteinuria and glomerulosclerosis. *Kidney Int*. 2006;69:2131-2147.
20. Matsusaka T, Xin J, Niwa S, et al. Genetic engineering of glomerular sclerosis in the mouse via control of onset and severity of podocyte-specific injury. *J Amer Soc Nephrol*. 2005;16:1013-1023.
21. Macary G, Rossert J, Bruneval P, et al. Transgenic mice expressing nitroreductase gene under the control of the podocin promoter. A new murine model of inductible glomerular injury. *Virchows Archiv*. 2010;456:325-337.
22. Kim YH, Goyal M, Kurnit D, et al. Podocyte depletion and glomerulosclerosis have a direct relationship in the PAN-treated rat. *Kidney Int*. 2001;60:957-968.
23. Wharram BL, Goyal M, Wiggins JE, et al. Podocyte depletion causes glomerulosclerosis. Diphtheria toxin-induced podocyte depletion in rats expressing human diphtheria toxin receptor transgene. *J Amer Soc Nephrol*. 2005;16:2941-2952.
24. Pandey G, Westhoff JH, Schaefer F, Gehrig J. A smart imaging workflow for organ-specific screening in a cystic kidney zebrafish disease model. *Internat J Mol Sci*. 2019;20:1290.
25. Westhoff JH, Steenbergen PJ, Thomas LSV, Heigwer J, Bruckner T, Cooper L, Tönshoff B, Hoffmann GF, Gehrig J In vivo High-Content Screening in Zebrafish for Developmental Nephrotoxicity of Approved Drugs, *Frontiers in Cell and Developmental Biology*. (2020; 8: 1–15. http://dx.doi.org/10.3389/fcell.2020.00583.
26. McKee RA, Wingert RA. Zebrafish renal pathology. Emerging models of acute kidney injury. *Curr Pathobiol Rep*. 2015;3:171-181.
27. Kato Y, Tonomura Y, Hanafusa H, Nishimura K, Fukushima T, Ueno M. Adult zebrafish model for screening drug-induced kidney injury. *Toxicol Sci*. 2020;174:241-253.
28. Kriz W, Lemley KV. A potential role for mechanical forces in the detachment of podocytes and the progression of CKD. *J Amer Soc Nephrol*. 2015;26:258-269.
29. Endlich K, Kliewe F, Endlich N. Stressed podocytes-mechanical forces, sensors, signaling and response. *Pflugers Arch*. 2017;469:937-949.
30. Kriz W, Hähnel B, Hosser H, Rösener S, Waldherr R. Structural analysis of how podocytes detach from the glomerular basement membrane under hypertrophic stress. *Front Endocrinol*. 2014;5:207.
31. Neal CR, Crook H, Bell E, Harper SJ, Bates DO. Three-dimensional reconstruction of glomeruli by electron microscopy reveals a distinct restrictive urinary subpodocyte space. *J Amer Soc Nephrol*. 2005;16:1223-1235.
32. Smeets B, Te Loeke NAJM, Dijkman HBPM, et al. The parietal epithelial cell. A key player in the pathogenesis of focal segmental glomerulosclerosis in Thy-1.1 transgenic mice. *J Amer Soc Nephrol*. 2004;15:928-939.
33. Holderied A, Romoli S, Eberhard J, et al. Glomerular parietal epithelial cell activation induces collagen secretion and thickening of Bowman's capsule in diabetes. *Lab Invest*. 2015;95:273-282.
34. Ohtaka A, Ootaka T, Sato H, et al. Significance of early phenotypic change of glomerular podocytes detected by Pax2 in primary focal segmental glomerulosclerosis. *Am J Kidney Dis*. 2002;39:475-485.
35. Dijkman H, Smeets B, van der Laak J, Steenbergen E, Wetzels J. The parietal epithelial cell is crucially involved in human idiopathic focal segmental glomerulosclerosis. *Kidney Int*. 2005;68:1562-1572.
36. Suzuki T, Matsusaka T, Nakayama M, et al. Genetic podocyte lineage reveals progressive podocytopenia with parietal cell hyperplasia in a murine model of cellular/collapsing focal segmental glomerulosclerosis. *Amer J Pathol*. 2009;174:1675-1682.
37. Appel D, Kershaw DB, Smeets B, et al. Recruitment of podocytes from glomerular parietal epithelial cells. *J Amer Soc Nephrol*. 2009;20:333-343.
38. Eng DG, Sunseri MW, Kaverina NV, Roeder SS, Pippin JW, Shankland SJ. Glomerular parietal epithelial cells contribute to adult podocyte regeneration in experimental focal segmental glomerulosclerosis. *Kidney Int*. 2015;88:999-1012.
39. Nagata M. Podocyte injury and its consequences. *Kidney Int*. 2016;89:1221-1230.
40. Romoli S, Angelotti ML, Antonelli G, et al. CXCL12 blockade preferentially regenerates lost podocytes in cortical nephrons by targeting an intrinsic podocyte-progenitor feedback mechanism. *Kidney Int*. 2018;94:1111-1126.

41. Kuppe C, Gröne H-J, Ostendorf T, et al. Common histological patterns in glomerular epithelial cells in secondary focal segmental glomerulosclerosis. *Kidney Int*. 2015;88:990-998.
42. Yin C, Evason KJ, Maher JJ, Stainier DYR. The basic helix-loop-helix transcription factor, heart and neural crest derivatives expressed transcript 2, marks hepatic stellate cells in zebrafish. Analysis of stellate cell entry into the developing liver. *Hepatology*. 2012;56:1958-1970.
43. Poss KD, Wilson LG, Keating MT. Heart regeneration in zebrafish. *Science*. 2002;298:2188-2190.
44. Steenbergen PJ, Heigwer J, Pandey G, Tönshoff B, Gehrig J, Westhoff JH. A multiparametric assay platform for simultaneous in vivo assessment of pronephric morphology, renal function and heart rate in larval zebrafish. *Cells*. 2020;9:1269.

SUPPORTING INFORMATION

Additional supporting information may be found online in the Supporting Information section.

How to cite this article: Ursula Ingeborg Hansen K, Siegerist F, Daniel S, et al. Prolonged podocyte depletion in larval zebrafish resembles mammalian focal and segmental glomerulosclerosis. *The FASEB Journal*. 2020;34:15961–15974. https://doi.org/10.1096/fj.202000724R